Chiral Majorana interference as a source of quantum entanglement

Luca Chirolli,[1,*] José Pablo Baltanás,[2] and Diego Frustaglia[2]
[1]*Fundación IMDEA Nanoscience, E-28049 Cantoblanco Madrid, Spain*
[2]*Departamento de Física Aplicada II, Universidad de Sevilla, E-41012 Sevilla, Spain*

(Received 18 January 2018; published 17 April 2018)

Two-particle Hanbury Brown–Twiss interferometry with chiral Majorana modes produces maximally entangled electron-hole pairs. We promote the electron-hole quantum number to an interferometric degree of freedom and complete the set of linear tools for single- and two-particle interferometry by introducing a key phase gate that, combined with a Mach-Zehnder, allows full electron-hole rotations. By considering entanglement witnesses built on current cross-correlation measurements, we find that the possibility of independent local-channel rotations in the electron-hole subspace leads to a significant boost of the entanglement detection power.

DOI: 10.1103/PhysRevB.97.155416

I. INTRODUCTION

Entanglement is at the core of quantum theory and represents a key resource for quantum information and computation. Generation, manipulation, and detection of entangled electrons is at the basis of quantum computing with integrated solid-state devices. A great amount of attention has been devoted to entanglement generation in multiterminal mesoscopic conductors, with most noticeable schemes relying on Cooper pair emission from superconducting contacts [1,2], correlated electron-hole (e-h) entangled states by tunnel barriers [3], and integrated single-particle emitters [4] (see Refs. [5,6] for a review). Detection of entangled fermions in the context of quantum transport was first proposed as a particular consequence of antibunching in current cross-correlation measurements for a subclass of states (spin-entangled particles propagating along different channels) by using a beam splitter (BS) analyzer [7–9]. This was later generalized to the case of multiple mode and occupancy entanglement [10–12], where current cross correlations can provide entanglement witnesses [13,14].

Here, we suggest the use of chiral Majorana modes (χMMs) as a tool for the generation, manipulation, and detection of entanglement in the *e-h* and *channel* degree of freedom (DoF) in multiterminal platforms. This is done by integrating setups proposed in the literature, such as Mach-Zehnder (MZ) [15,16] and Hanbury Brown–Twiss (HBT) [17,18] interferometers, together with a phase gate. The latter permits the implementation of an energy-independent phase shift between electron and hole states. Most importantly, the combined action of a MZ and a phase gate allows for arbitrary rotations in the e-h DoF and to perform local operations in each propagating channel.

The advantage of using chiral Majorana channels is twofold. On the one hand, two-particle interferometry in topological superconductors (TSCs) hosting χMMs at their boundary [19] produces superpositions of maximally entangled states. In particular, as pointed out in Ref. [17], postselecting states with one fermion per lead yields maximally entangled pairs in the electron-hole space. This *guarantees* the production of exactly maximally entangled states. On the other hand, the possibility to arbitrarily rotate the state in the e-h DoF independently in each channel allows for measurements of the e-h state in any basis, boosting the power of the entanglement witness far beyond the limits of the proposals with ordinary particle currents. Our approach makes it possible to exploit single- and two-particle interferometry in the e-h DoF as a platform for quantum computation in dual-rail architectures [20,21].

Our proposal can be easily generalized to ordinary electrons and holes in hybrid normal/superconductor heterostructures. Interferometry in the e-h DoF is in principle possible with chiral channels in contact with a superconductor [22–25], where e-h superpositions copropagate in the same channel, in analogy with copropagating spin-resolved edge states in the integer quantum Hall effect (IQHE) [26–29]. Recent experiments with chiral one-dimensional (1D) channels in contact with *s*-wave superconductors opened the way to exploring Andreev reflection on 1D chiral channels [23,25]. At the same time, no proposal for controlled BS, MZ, or HBT e-h interferometers is currently available with ordinary superconductors.

The paper is structured as follows: in Sec. II we describe the system under study, characterized by Dirac and Majorana edge channels; in Sec. III we describe the interferometric setup, by reviewing interferometric elements proposed in the literature and by introducing a fundamental phase gate; in Sec. IV we assess the presence of entanglement in the output channels by studying the current cross correlations and their relation to entanglement witnesses, showing how the possibility to perform independent local-channel rotations in the e-h subspace greatly enhances the entanglement detection power. In Sec. V we conclude the work with a summary of the results.

II. THE SYSTEM

The main ingredients are chiral Dirac modes (χDMs) and χMMs in quantum anomalous Hall insulator/SC structures, as those proposed in Refs. [15,16]. The recent experimental detection of χMMs in these systems [30,31] makes the present

*luca.chirolli@imdea.org

proposal feasible and particularly appealing. The system consists in the two-dimensional (2D) surface of a topological insulator (TI) on top of a substrate divided in ferromagnetic (FM) and SC regions. The TI surface hosts a single 2D fermionic Dirac cone described by $H_0 = -iv(\nabla \times \mathbf{s})_z$, with $\mathbf{s}$ a vector of spin Pauli matrices. A FM domain wall acts as $H_{\rm fm} = M(\mathbf{r})s_z$ and gaps the system everywhere apart from a line where the domain wall changes sign. Along this line a 1D χDM forms, analogous to the edge states of the IQHE, and can be used as an electronic waveguide. Similarly, SC proximity induces singlet pairing described by $H_{\rm SC} = \Delta \sum_{\mathbf{k}} c^\dagger_{\mathbf{k},\uparrow} c^\dagger_{-\mathbf{k},\downarrow} + \text{H.c}$ that opens a topological gap, thus realizing a 2D TSC. Gapless χMMs form along the border between the SC and the FM regions. By properly arranging these regions it is possible to realize an interferometric setup composed by several linear elements. We now characterize the transport in terms of scattering matrices in the Landauer-Büttiker formalism adapted to describe χMMs [32].

III. INTERFEROMETRIC SETUP

The setup is illustrated in Fig. 1. We follow the notation of Ref. [17] and denote χDMs with double arrow lines and χMMs with single arrow lines. Given that χDMs have $\langle s_y \rangle = -1$, we can regard the fundamental excitations as spinless Dirac fermions described by fermionic operators $a(\epsilon)$ at energy ϵ. For energies $0 < \epsilon \ll \Delta$ we define electron- and holelike states in channel i at energy ϵ as $a_{i,+}(\epsilon) = a_i(\epsilon)$ and $a_{i,-}(\epsilon) = a_i^\dagger(-\epsilon)$, and introduce an e-h DoF $\tau = \pm 1 = e,h$. Analogously, at the boundary of the TSC a single χMM flows, either clockwise $\gamma_1(\epsilon)$ at the boundary between the TSC and the $M_\uparrow$ magnetic domain, or anticlockwise $\gamma_2(\epsilon)$ at the boundary between the TSC and the $M_\downarrow$ magnetic domain.

Current is injected in the system upon biasing contacts 1 and 2 and it is collected in contacts 3 and 4, that are kept grounded. The resulting current and noise in contacts 3 and 4 can be obtained in terms of unitary scattering matrices S relating incoming Dirac modes $a_{j,\sigma}$ to outgoing Dirac modes $b_{i,\tau}$,

$$b_{i,\tau}(\epsilon) = \sum_{j=1,2;\sigma=\pm} S_{i,\tau;j,\sigma}(\epsilon) a_{j,\sigma}(\epsilon). \tag{1}$$

Particle-hole symmetry implies $S(\epsilon) = \tau_x S^*(-\epsilon)\tau_x$.

The setup in Fig. 1 is characterized by four kinds of linear elements: (i) a BS, (ii) a MZ interferometer, (iii) a phase shifter, and (iv) a four-terminal element. Additionally, an ordinary quantum point contact (QPC) is introduced to mix χDMs, in analogy with interferometry in the IQHE edge states [33]. Some of these elements have been suggested in the literature, so that we here review them in the spirit of two-particle interferometry.

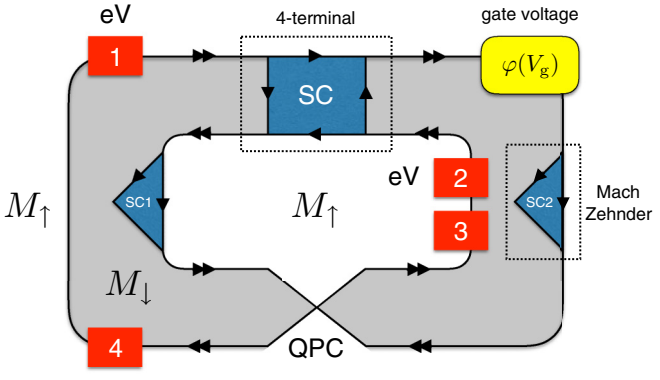

FIG. 1. Setup: a domain wall on top of a TI 2D surface state generates χDMs (double arrows) and an s-wave SC opens a topological gap, at whose boundary with the domain wall χMMs form (single arrow). Carriers are injected into the system by biasing contacts 1 and 2 and go first through the four-terminal device, which acts as a two-particle interferometer. The outgoing carriers then undergo local operations through phase shifts and MZs and collide into a QPC that mixes the channels. Currents and correlations are measured in contacts 3 and 4. The MZs and phase shifts can be also placed after the QPC.

A. Beam splitter

In this context, we denote a BS as an element that takes an incoming χDM and produces two outgoing χMMs. The trijunction between a magnetic domain wall and a TSC forces the incoming electron a_+ and hole a_- states to split into two χMMs, γ_1 and γ_2 [15,16]. For energies much smaller than the SC gap, we can assume the BS scattering matrix to be energy independent, reading [15,16]

$$\begin{pmatrix} \gamma_1(\epsilon) \\ \gamma_2(\epsilon) \end{pmatrix} = \frac{1}{\sqrt{2}} \begin{pmatrix} 1 & 1 \\ i & -i \end{pmatrix} \begin{pmatrix} a_+(\epsilon) \\ a_-(\epsilon) \end{pmatrix}. \tag{2}$$

B. Mach-Zehnder

By combing two BSs separated by a region where the two χMMs propagate along two paths of different length one can realize a MZ interferometer for electrons and holes described by [15,16,34]

$$\begin{pmatrix} a_+ \\ a_- \end{pmatrix}_R = S_{\rm BS}^\dagger \begin{pmatrix} e^{i\pi n_v + ikL_1} & 0 \\ 0 & e^{ikL_2} \end{pmatrix} S_{\rm BS} \begin{pmatrix} a_+ \\ a_- \end{pmatrix}_L, \tag{3}$$

where $k(L_1 - L_2) = \epsilon \delta L / v_M$ is the phase difference gathered at energy ϵ and n_v is the number of vortices in the SC, with v_M the velocity of the χMMs. The scattering matrix thus mixes incoming chiral electron and hole states in the left (L) lead to outgoing chiral electron and hole states in the right (R) lead. At finite energy, by varying the path length difference δL it is possible to perform arbitrary rotations around the τ_x axis between incoming and outgoing states in a given channel. At zero energy this element is expressed as a τ_x scattering matrix in the e-h space, that represents a $\mathbb{Z}_2$ MZ interferometer being able only to change an electron into a hole, and vice versa.

C. Phase shifter

A fundamental ingredient appearing in the setup of Fig. 1 is the phase shifter between electrons and holes in a given Dirac channel. This can be easily accomplished by a top gate that locally shifts the chemical potential. For a gate voltage V_g such that $|V_g| \ll M$, where M is the magnitude of the Zeeman splitting of the magnetic domains, electrons and holes will in general acquire an opposite phase,

$$a_+(\epsilon) \to e^{i\varphi_g} a_+(\epsilon), \qquad a_-(\epsilon) \to e^{-i\varphi_g} a_-(\epsilon), \tag{4}$$

with $\varphi_g = (e/v)\int_0^L dx\, V_g(x)$. Importantly, this phase is energy independent so that also carriers at $\epsilon = 0$ acquire it. The scattering matrix associated to the phase shift realizes a phase gate

$$P = \exp(i\varphi_g \tau_z). \tag{5}$$

This element is of paramount importance in that, combined with the MZ, it provides a way to rotate the states in the e-h space and generate any superposition state. Moreover, a channel-dependent shift can be obtained by modifying the path length of a given channel. This can be achieved by moving the domain wall through a magnetic field.

D. Four-terminal element

Finally, the core of the setup in Fig. 1 is a four-terminal device that mixes two incoming χDMs into two outgoing χDMs. In terms of electron and hole channels, the element mixes four incoming states into four outgoing states. This four-terminal element was introduced in Refs. [15,17] and it is described by the scattering matrix

$$\begin{pmatrix} b_{1+} \\ b_{1-} \\ b_{2+} \\ b_{2-} \end{pmatrix} = \frac{1}{2}\begin{pmatrix} 1 & 1 & 1 & 1 \\ 1 & 1 & -1 & -1 \\ 1 & -1 & -\eta & \eta \\ 1 & -1 & \eta & -\eta \end{pmatrix}\begin{pmatrix} a_{1+} \\ a_{1-} \\ a_{2+} \\ a_{2-} \end{pmatrix}, \tag{6}$$

with $\eta = (-1)^{n_v} e^{i\epsilon\delta L/\hbar v_M}$ a phase due to the propagation of the χMMs in the interferometer (here δL is the path length difference between the two-particle trajectories [15,17]). At zero energy the phase can be only $\eta = \pm 1$, depending on the number of vortices n_v in the system. A more generic four-terminal element can be obtained by allowing for a cross talk between the χMMs in the SC region.

IV. CROSS CORRELATIONS AS ENTANGLEMENT WITNESSES

The general idea developed in Refs. [7–11] is that, given an unknown initial state that is possibly entangled in the e-h and channel DoF, it is possible to establish the presence of entanglement via measuring current cross correlations after mixing the channels through a QPC and relate the cross correlator to an entanglement witness. We now show that witnessing entanglement in an e-h system is not only possible, but also much more effective, thanks to the possibility to insert MZs before and after the QPC.

The most general unknown two-particle state at the input of the QPC can be cast in the generic form

$$|\Psi\rangle = \sin\theta(\cos\phi|\Phi_{11}\rangle + \sin\phi|\Phi_{22}\rangle) + \cos\theta|\Phi_{12}\rangle, \tag{7}$$

with $\theta,\phi \in [0,\pi/2]$ and $|\Phi_{ij}\rangle$ two-particle states at energy ϵ in leads i and j, $|\Phi_{ij}\rangle = \sum_{\alpha,\beta}\Phi^{(ij)}_{\alpha,\beta} a^\dagger_{i,\alpha}(E) a^\dagger_{j,\beta}(E)|0\rangle$, where $|0\rangle$ is the grounded Fermi sea. The states satisfy $\Phi^{(jj)}_{\alpha,\beta} = -\Phi^{(jj)}_{\beta,\alpha}$ and the normalization conditions $\sum_{\alpha,\beta}|\Phi^{(12)}_{\alpha,\beta}|^2 = 1$ and $\sum_{\alpha,\beta}|\Phi^{(jj)}_{\alpha,\beta}|^2 = 1/2$. The state described by Eq. (7) displays entanglement in the *occupation number* and *channel* DoF [35,36].

Before the QPC, we induce a phase difference between the electron and hole in each channel by local gate voltages and domain-wall displacement. For the moment we do not consider the MZs that are present in the setup of Fig. 1. The QPC mixes the channel of the incoming particles without changing the electron/hole character of the particle injected. The outgoing states after the combined system phase shifter plus QPC is given by $b_{j,\tau} = \sum_{j'=1,2} S^\tau_{j,j'} a_{j',\tau}$, where $b_{j,\tau}$ are the outgoing states after the QPC in lead j with electron/hole character τ, where the scattering matrix is given by

$$S^\tau = \begin{pmatrix} r & t' e^{i\varphi_\tau} \\ t & r' e^{i\varphi_\tau} \end{pmatrix}. \tag{8}$$

The phase φ_τ accumulated before the QPC has two contributions: the gate contribution φ_g, which is opposite for electrons and holes, and a dynamical phase difference due to the different path length between the four-terminal scattering region and the QPC along the two possible paths. This contribution is the same for electrons and holes, so that we can write $\varphi_\tau = \varphi_L + \tau\varphi_g$, with $\varphi_L = \epsilon\delta L/v$ and v the velocity of Dirac modes. We now consider the dimensionless current cross correlator between the output channels 3 and 4,

$$C_{34} \equiv \frac{h^2\nu^2}{2e^2}\lim_{\mathcal{T}\to\infty}\int_0^{\mathcal{T}}\frac{dt_1 dt_2}{\mathcal{T}^2}\langle I_3(t_1) I_4(t_2)\rangle, \tag{9}$$

where $\mathcal{T}$ is the measurement time. The current operator of chiral fermions in lead i is written in terms of electron and hole contributions as

$$I_i(t) = \frac{e}{h\nu}\sum_{\epsilon,\omega,\tau=\pm} e^{-i\omega t}\tau b^\dagger_{i,\tau}(\epsilon) b_{i,\tau}(\epsilon+\hbar\omega), \tag{10}$$

and the average $\langle\cdots\rangle$ is taken over the incoming state by assuming a discrete spectrum characterized by a density of states ν in each lead. Importantly, electrons and holes contribute with different sign to the current, which is accounted for by the τ in Eq. (10). In each lead there are incoming and outgoing states. However, due to the chirality of states localized at the domain-wall boundary, there is no backscattering and the current can be described only in terms of outgoing channels.

The quantity C_{34} has the advantage of being a linear function of the input state [11]. Assuming a QPC characterized by $r' = r = \sqrt{1-T}$ and $t' = t = i\sqrt{T}$, with T the transmission probability of the QPC we find

$$C_{34}(\Psi) = T(1-T)[w\cos^2\theta - \sin^2\theta + v\sin^2\theta\sin(2\phi)] + \frac{1}{2}\cos^2\theta\sum_{\tau\sigma}\tau\sigma\left|\Phi^{(12)}_{\tau,\sigma}\right|^2, \tag{11}$$

where v and w are real quantities satisfying $|v|,|w| \leqslant 1$ that can be expressed in terms of the phases φ_τ as

$$v = 2\mathrm{Re}\sum_{\tau,\sigma}\left(\Phi^{(11)}_{\tau,\sigma}\right)^*\Phi^{(22)}_{\sigma,\tau}e^{i\varphi_\tau + i\varphi_\sigma}, \tag{12}$$

$$w = \sum_{\tau,\sigma}\sigma\tau\left(\Phi^{(12)}_{\tau,\sigma}\right)^*\Phi^{(12)}_{\sigma,\tau}e^{i(\varphi_\tau-\varphi_\sigma)}. \tag{13}$$

The correlator C_{34} is very similar to that of Ref. [11]. Antisymmetry of the $|\Phi_{jj}\rangle$ states implies that φ_g drops from v. Analogously, the phase φ_L drops from w. By further redefining $\varphi_g \to \pi/2 + \varphi_g$ we have that $w = \sum_{\tau,\sigma}(\Phi^{(12)}_{\tau,\sigma})^*\Phi^{(12)}_{\sigma,\tau}e^{i\varphi_g(\tau-\sigma)}$.

As a particular case we consider incoming states with singly occupied channels 1 and 2 by choosing $\theta = 0$ in the generic input state (7). The current correlator is found to be

$$C_{34}(\Phi_{12}) = \frac{1}{2}\sum_{\tau\sigma} \tau\sigma |\Phi^{(12)}_{\tau,\sigma}|^2 + T(1-T)w. \quad (14)$$

The quantity w captures all the relevant information on the input state. One can show that w is non-negative for separable input states [10]. The first term in Eq. (14) is nothing but the cross correlator before the QPC, $C_{12}(\Phi_{12}) = \frac{1}{2}\sum_{\tau\sigma} \tau\sigma |\Phi^{(12)}_{\tau\sigma}|^2$. Experimentally one can act on the QPC and switch the tunneling between counterpropagating states on and off (by setting $T = 0$ or $T = 1$) and measure separately $C_{34}(\Phi_{12})$ and $C_{12}(\Phi_{12})$. It then follows that the case $C_{34}(\Phi_{12}) - C_{12}(\Phi_{12}) < 0$ witnesses the presence of entanglement in the state $|\Phi_{12}\rangle$.

For $\theta \neq 0$, i.e., incoming channels 1 and 2 with fluctuating local occupancy in (7), $C_{34}(\Psi)$ can be related to the entanglement of formation $E_f(\Psi)$ [37]: generalized Werner states [38,39] are defined by introducing a joint orthonormal basis for ports 1 and 2 formed by states $|\chi_k\rangle_1 \otimes |\chi_k\rangle_2$ and $|\Psi^{(\pm)}_{kk'}\rangle = (|\chi_k\rangle_1 \otimes |\chi_{k'}\rangle_2 \pm |\chi_{k'}\rangle_1 \otimes |\chi_k\rangle_2)/\sqrt{2}$ with $k < k'$, where k enumerates all configurations with two or fewer particles per port. It then follows that the entanglement of formation of a state ρ can be lower bounded by the quantity $W(\rho) = \sum_{kk'} \langle\Psi^{(-)}_{kk'}|\rho|\Psi^{(-)}_{kk'}\rangle/2$. Analogously, we can relate the net correlator

$$\delta C_{34}(\Psi) \equiv C_{34}(T = 1/2) - C_{34}(T = 0) \quad (15)$$

$$= C_{34}(\Psi) - C_{12}(\Psi), \quad (16)$$

which depends only on the quantities v, w, and the angle θ, to a lower bound to the entanglement of formation through

$$W(\Psi) = -2\delta C_{34}(\Psi) + \cos^2(\theta)/2. \quad (17)$$

By noticing that $W(\Psi) > -2\delta C_{34}(\Psi)$ we find that $W(\Psi) > 1/2$ and, consequently, $E_f(\Psi) > 0$ whenever $\delta C_{34}(\Psi) < -1/4$ (see Refs. [10,11]). Thus, the sign of $-2\delta C_{34}(\Psi) - 1/2$ is sufficient to witness the presence of entanglement in the initial state Ψ. We can further postprocess the data and obtain full information about the state. First of all, we use that $v(\varphi_L + \pi/2) = -v(\varphi_L)$. This allows one to define $\delta C^{(\pm)}_{34} = [\delta C_{34}(\varphi_L + \pi/2) \pm \delta C_{34}(\varphi_L)]/2$ such that

$$\delta C^{(+)}_{34}(\varphi_g) = [w(\varphi_g)\cos^2\theta - \sin^2\theta]/4, \quad (18)$$

$$\delta C^{(-)}_{34}(\varphi_L) = v(\varphi_L)\sin^2\theta\ \sin(2\phi)/4. \quad (19)$$

We then notice that $\cos^2\theta = 2C_{12}(\Psi)/(2\bar{w} - 1)$, where $\bar{w} = \int \frac{d\varphi_g}{2\pi} w(\varphi_g)$. Upon introducing

$$\delta\bar{C}^{(+)}_{34} = \int \frac{d\varphi_g}{2\pi}\delta C^{(+)}_{34}(\varphi_g) = \frac{1}{4}[(1+\bar{w})\cos^2\theta - 1], \quad (20)$$

we can express

$$\cos^2\theta = \tfrac{2}{3}(4\delta\bar{C}^{(+)}_{34} - C_{12} + 1), \quad (21)$$

allowing one to establish the occupation and channel admixture as a function of measurable quantities. Finally, we notice that the states $|\Phi_{jj}\rangle$ can only be e-h singlets, so that v depends only on the relative phase difference between Φ_{11} and Φ_{22}. By varying φ_L one can then access $\sin(2\phi) = 2(\max_{\varphi_L}\delta C^{-}_{34} - \min_{\varphi_L}\delta C^{-}_{34})/(1-\cos^2\theta)$. The analysis allows one to fully access the occupation-number (e-h) and channel DoF entanglement by further exploiting the phase before the QPC [11]. This result can be generalized to generic mixed input states ρ, as the combination of the maps C_{12} and C_{34} preserves the linearity of δC_{34}.

A. HBT state

Having established the general entanglement witnessing protocol via current cross-correlation measurements, we now apply it to the output state of the two-particle interferometer in the setup of Fig. 1. Upon biasing only the contacts 1 and 2 the incoming state at energy ϵ reads $|\Psi_\epsilon\rangle_{\rm in} = a^\dagger_{1+}(\epsilon)a^\dagger_{2+}(\epsilon)|0\rangle$ and the outgoing state reads $|\Psi_\epsilon\rangle_{\rm out} = S_{j,\mu;1,+}S_{k,\nu;2,+}b^\dagger_{j,\mu}(\epsilon)b^\dagger_{k,\nu}(\epsilon)|0\rangle$ (summed over repeated indexes), with S the scattering matrix in Eq. (6). In Ref. [17] the system was studied as a HBT two-particle interferometer and it was recognized that postselecting states with a single fermion per lead yields maximally entangled states. In this case the current cross correlations allows one to access $v = -{\rm Re}[\eta e^{2i\varphi_L}]$ and $w = \{[1 + \cos(2\varphi_g)] + {\rm Re}[\eta][1 - \cos(2\varphi_g)]\}/2$, and the associated witness for $T = 1/2$ and η real is

$$W(\Psi_{\rm HBT}) = \tfrac{1}{8}[3 - \eta + 2\eta\ \cos(2\varphi_L) - (1-\eta)\cos(2\varphi_g)]. \quad (22)$$

In particular, for $\eta = -1$, $\varphi_L = \pi/2$, and $\varphi_g = \pi/2$ one can reach $W = 1$, which corresponds to $E_f = 1$. This means that the phases are means to rotate the initial state to have maximum overlap with the generalized Werner states, confirming that the state coming out from the HBT interferometer is a superposition of maximally entangled states.

B. Local operations

The quantity C_{34} differs from that of Ref. [11] in the measured observable: particle current in the original case in contrast to charge current in the present case. This grants a much more powerful characterization of the incoming states. By inserting MZs before the QPC we can rotate the e-h state on each channel and measure any linear combination of the three Pauli matrices τ_i, with $i = 1,2,3$. This operation only affects the state $|\Phi_{12}\rangle$ (the states $|\Phi_{jj}\rangle$ are e-h singlets, so that any single-particle rotation can only affect the global phase of the state $|\Phi_{jj}\rangle$) and C_{12} measurements can assess every local single-particle observable. The insertion of MZs and phase shifters together with the possibility of switching the QPC on and off give us the opportunity to cross correlate the local operation and to perform a full tomography of the input state.

V. CONCLUSIONS

In this work we suggest to use interferometry with chiral Majorana modes to generate, manipulate, and detect quantum entanglement in the electron-hole and channel degrees of freedom in multiterminal hybrid normal-superconductor platforms. A fundamental two-particle Hanbury Brown–Twiss interferometer previously proposed in the literature allows one to generate maximally entangled pairs in the electron-hole degree of freedom. We integrate a set of single-particle elements, such as beam splitters and Mach-Zehnder interferometers, with

a fundamental phase gate that allows one to generate a phase difference between electron and hole at zero energy and that, combined with the $\mathbb{Z}_2$ Mach-Zehnder interferometer, allows full rotation in the e-h space. Entanglement in the output states is detected through the assessment of entanglement witnesses by means of current cross-correlation measurements, extended to the case of particle-hole current carrying states.

The completion of the set of single-particle and two-particle linear elements allows one to perform any operation in the e-h degree of freedom and to fully manipulate quantum states encoded in this platform. The possibility to perform independent local-channel rotations in the e-h subspace greatly enhances the entanglement detection power and makes electron-hole systems an ideal platform for quantum computation in dual-rail architectures.

Note added. Recently, B. Lian *et al.* [40] independently studied chiral Majorana modes on a similar Corbino geometry.

ACKNOWLEDGMENTS

The authors are thankful to F. Taddei, V. Giovannetti, and C. W. J. Beenakker for very useful discussions. L.C. acknowledges funding from the European Union's Seventh Framework Programme (FP7/2007-2013) through the ERC Advanced Grant NOVGRAPHENE (GA Grant No. 290846) and the Comunidad de Madrid through the grant MAD2D-CM, Grant No. S2013/MIT-3007. D.F. and J.P.B. acknowledge support from Projects No. FIS2014-53385-P and No. FIS2017-86478-P (MINECO/FEDER, Spain).

[1] P. Recher, E. V. Sukhorukov, and D. Loss, Phys. Rev. B **63**, 165314 (2001).
[2] G. B. Lesovik, T. Martin, and G. Blatter, Eur. Phys. J. B **24**, 287 (2001).
[3] C. W. J. Beenakker, C. Emary, M. Kindermann, and J. L. van Velsen, Phys. Rev. Lett. **91**, 147901 (2003).
[4] J. Splettstoesser, M. Moskalets, and M. Büttiker, Phys. Rev. Lett. **103**, 076804 (2009).
[5] C. W. J. Beenakker, in *Quantum Computers, Algorithms, and Chaos*, in Proceedings of the International School of Physics "Enrico Fermi" - Varenna, edited by P. Z. G. Casati and D. L. Shepelyansky (IOS Press Ebooks, Amsterdam, 2006).
[6] G. Burkard, in *Handbook of Theoretical and Computational Nanotechnology 3*, edited by M. Rieth and W. Schommers (American Scientific Publishers, Valencia, CA, 2004).
[7] G. Burkard, D. Loss, and E. V. Sukhorukov, Phys. Rev. B **61**, R16303 (2000).
[8] F. Taddei and R. Fazio, Phys. Rev. B **65**, 075317 (2002).
[9] G. Burkard and D. Loss, Phys. Rev. Lett. **91**, 087903 (2003).
[10] V. Giovannetti, D. Frustaglia, F. Taddei, and R. Fazio, Phys. Rev. B **74**, 115315 (2006).
[11] V. Giovannetti, D. Frustaglia, F. Taddei, and R. Fazio, Phys. Rev. B **75**, 241305 (2007).
[12] J. P. Baltanás and D. Frustaglia, J. Phys.: Condens. Matter **27**, 485302 (2015).
[13] M. Horodecki, P. Horodecki, and R. Horodecki, Phys. Lett. A **223**, 1 (1996).
[14] M. Lewenstein, B. Kraus, J. I. Cirac, and P. Horodecki, Phys. Rev. A **62**, 052310 (2000).
[15] L. Fu and C. L. Kane, Phys. Rev. Lett. **102**, 216403 (2009).
[16] A. R. Akhmerov, J. Nilsson, and C. W. J. Beenakker, Phys. Rev. Lett. **102**, 216404 (2009).
[17] G. Strübi, W. Belzig, M.-S. Choi, and C. Bruder, Phys. Rev. Lett. **107**, 136403 (2011).
[18] S. B. Chung, X.-L. Qi, J. Maciejko, and S.-C. Zhang, Phys. Rev. B **83**, 100512 (2011).
[19] C. W. J. Beenakker, Annu. Rev. Condens. Matter Phys. **4**, 113 (2013).
[20] I. L. Chuang and Y. Yamamoto, Phys. Rev. A **52**, 3489 (1995).
[21] E. Knill, R. Laflamme, and G. J. Milburn, Nature (London) **409**, 46 (2001).
[22] H. Hoppe, U. Zülicke, and G. Schön, Phys. Rev. Lett. **84**, 1804 (2000).
[23] P. Rickhaus, M. Weiss, L. Marot, and C. Schönenberger, Nano Lett. **12**, 1942 (2012).
[24] D. J. Clarke, J. Alicea, and K. Shtengel, Nat. Phys. **10**, 877 (2014).
[25] G.-H. Lee, K.-F. Huang, D. K. Efetov, D. S. Wei, S. Hart, T. Taniguchi, K. Watanabe, A. Yacoby, and P. Kim, Nat. Phys. **13**, 693 (2017).
[26] B. Karmakar, D. Venturelli, L. Chirolli, F. Taddei, V. Giovannetti, R. Fazio, S. Roddaro, G. Biasiol, L. Sorba, V. Pellegrini *et al.*, Phys. Rev. Lett. **107**, 236804 (2011).
[27] L. Chirolli, D. Venturelli, F. Taddei, R. Fazio, and V. Giovannetti, Phys. Rev. B **85**, 155317 (2012).
[28] L. Chirolli, F. Taddei, R. Fazio, and V. Giovannetti, Phys. Rev. Lett. **111**, 036801 (2013).
[29] B. Karmakar, D. Venturelli, L. Chirolli, V. Giovannetti, R. Fazio, S. Roddaro, L. N. Pfeiffer, K. W. West, F. Taddei, and V. Pellegrini, Phys. Rev. B **92**, 195303 (2015).
[30] J. Wang, Q. Zhou, B. Lian, and S.-C. Zhang, Phys. Rev. B **92**, 064520 (2015).
[31] Q. L. He, L. Pan, A. L. Stern, E. C. Burks, X. Che, G. Yin, J. Wang, B. Lian, Q. Zhou, E. S. Choi *et al.*, Science **357**, 294 (2017).
[32] J. Li, G. Fleury, and M. Büttiker, Phys. Rev. B **85**, 125440 (2012).
[33] I. Neder, N. Ofek, Y. Chung, M. Heiblum, D. Mahalu, and V. Umansky, Nature (London) **448**, 333 (2007).
[34] M. Alos-Palop, R. P. Tiwari, and M. Blaauboer, Phys. Rev. B **89**, 045307 (2014).
[35] N. Schuch, F. Verstraete, and J. I. Cirac, Phys. Rev. Lett. **92**, 087904 (2004).
[36] H. M. Wiseman and J. A. Vaccaro, Phys. Rev. Lett. **91**, 097902 (2003).
[37] C. H. Bennett, D. P. DiVincenzo, J. A. Smolin, and W. K. Wootters, Phys. Rev. A **54**, 3824 (1996).
[38] K. G. H. Vollbrecht and R. F. Werner, Phys. Rev. A **64**, 062307 (2001).
[39] R. F. Werner, Phys. Rev. A **40**, 4277 (1989).
[40] B. Lian, X.-Q. Sun, A. Vaezi, X.-L. Qi, and S.-C. Zhang, arXiv:1712.06156.